metals

MDPI

Article

Interfacial Evolution and Shear Properties of Ultrasonic Spot-Welded Aluminum–Copper Joints with a Zn Interlayer

Tianwei Qiu [1,2], Qianqian Yu [1], Muhammed Nafis Osman Zahid [2,*], Daoyuan Li [3] and Qiang Chen [4]

[1] School of Mechanical Engineering, Shandong Huayu University of Technology, Dezhou 253034, China; 17685632649@163.com (T.Q.)
[2] Faculty of Manufacturing and Mechatronic Engineering Technology, Universiti Malaysia Pahang Al-Sultan Abdullah, Pekan 26600, Pahang, Malaysia
[3] School of Mechanical Engineering, Shandong University of Technology, Zibo 255000, China
[4] Department of Transportation Engineering, Dongying Technician College, Dongying 257092, China
* Correspondence: nafis@umpsa.edu.my

Abstract

Ultrasonic spot-welded 1060 Al/T2 Cu joints with a 0.1 mm Zn interlayer were examined through temperature measurements, microscopy, SEM/EDS, microhardness and shear testing to compare the responses to welding energy, Al thickness and post-weld holding. Increasing welding energy from 900 to 4000 J generally raised recorded peak temperatures and promoted growth of the relatively planar Cu–Zn-rich interfacial region and wavy Al–Zn-rich transition zone. In the 2 mm Al series, base-metal hardness decreased slightly, while composite near-interface hardness increased. For 2 mm Al, mean nominal shear strength reached 23.77 ± 6.70 MPa at 3000 J before decreasing at 4000 J. At the same programmed energy, 4 mm Al joints exhibited lower recorded temperatures and thinner interfacial regions; their mean strength increased throughout the tested range, reaching 20.50 ± 1.06 MPa at 4000 J. At 1400 J with 2 mm Al, Zn-assisted joints had a higher mean strength than the Zn-free control. Holding the 2 mm Al/1400 J joints at 250 °C promoted further interfacial growth, reduced the residual Zn region and increased composite near-interface hardness, while mean strength decreased to 8.23 ± 0.83 MPa after 3 h. Strengths are means ± sample standard deviations.

Keywords: ultrasonic spot welding; dissimilar aluminum–copper joining; Zn interlayer; interfacial microstructure; shear strength

Academic Editor: João Pedro Oliveira

Received: 12 November 2026
Revised: 23 November 2026
Accepted: 26 November 2026
Published: 28 November 2026

Copyright: © 2026 by the author. Licensee MDPI, Basel, Switzerland. This article is an open access article distributed under the terms and conditions of the Creative Commons Attribution (CC BY) license.

1. Introduction

Dissimilar Al/Cu joining is relevant to battery-tab and busbar assemblies because it combines aluminum and copper in an electrical connection. Joint assessment involves both load-bearing capacity and electrical resistance, and processing conditions suitable for one criterion may differ from those suitable for another [1]. Ultrasonic spot welding has been applied to multilayer Al foils and Cu tabs, where energy input and contact between layers influence weld quality [2]. During welding, interfacial motion and localized deformation progressively establish bonded regions. Using 1 mm Al and Cu sheets, Li et al. applied 20 kHz vibration, a 28 μm amplitude and a 700 N welding force, obtaining a mean tensile-shear failure-load plateau of 1663–1820 N after approximately 400 ms [3]. Grain and texture analyses have revealed asymmetric microstructural evolution, including recrystallization and subsequent grain growth on the Al side [4]. Increasing welding

time has also been associated with a higher microbond density, reduced remaining sheet thickness and lower mean hardness [5], while localized deformation and oxide-film fragmentation assist the formation of metal-to-metal contacts [6].

The development of these contacts involves changes in relative motion, local damage and interfacial structure. Laser Doppler vibrometry has resolved successive stages of relative motion during Al/Cu weld formation [7], and interface-geometry analyses have connected tensile-shear performance with the distribution of bonded regions and local damage conditions [8]. For 0.5 mm 1060 Al/T2 Cu sheets, Ma et al. described micro-weld formation, breakage and renewed attachment as welding progressed, reporting a maximum lap-shear failure load of 0.9 ± 0.03 kN at 0.29 s [9]. The structure of the resulting interface has also been examined using phase-sensitive techniques. In Al/Cu joints produced at 500 J, 30 psi and a 35 μm amplitude, Zhang et al. used TEM/HRTEM to identify an approximately 10 nm weld-generated transition layer containing amorphous material and nanocrystallines [10].

Processing conditions and specimen geometry influence both interfacial contact and deformation around the weld. In thin Al-tab/Cu-busbar specimens, indentation depth was particularly sensitive to welding time [11]. Tensile-shear and peel tests showed different responses to vibration amplitude [12], while comparisons of Al/Al, Al/Cu and Al/Ni joints identified material-dependent processing ranges [13]. Additional periodic force has been used to modify plastic deformation and interfacial bonding in Cu/Al ultrasonic welding [14]. Changes in plate thickness introduce further variations in the welding response. Al/Cu thickness comparisons have shown differences in temperature rise and fracture characteristics [15]. Müller et al. related workpiece geometry and natural frequencies to tool oscillation, power consumption and bond strength [16]. The influence of assembly geometry is also evident in multilayer joints, for which Sharma and Das reported different heat generation and T-peel loads between layer-wise and stacked fabrication [17].

Zn interlayers provide a means of modifying the interfacial configuration of Al/Cu ultrasonic joints. Balasundaram et al. used a 50 μm Zn foil between 1.5 mm Al5754-O and 1 mm C110 Cu and reported lap-shear tensile strengths 25–170% above those of the corresponding joints without Zn [18]. A non-monotonic strength response to welding energy has already been reported for Zn-assisted Al/Cu joints. Li et al. obtained a load of approximately 1450 N at 700 J, as estimated from Figure 9 in Ref. [19]. Comparisons of Ni, Zn and Mg interlayers showed that interlayer material and thickness influence joint morphology and failure behavior [20]. For Ni-foil joints, welding pressure and duration require coordinated adjustment [21], whereas ultrasonic-assisted joining with a SAC307 + Zn composite interlayer introduces additional Sn-based constituents and external heating [22]. The previous demonstrations of Zn-assisted bonding motivate the choice of pure Zn for the present comparison. A 0.1 mm foil was held constant across the welding-energy, Al-thickness and post-weld holding series so that the same interlayer configuration could be examined under different processing histories. Interlayer material and foil thickness were not optimized. Ni-based and nanoscale interlayers would introduce additional composition or length-scale variables and were outside the scope of this comparison.

Thermal exposure after welding extends interfacial evolution beyond the period of ultrasonic vibration. Ao et al. reported increasing intermetallic-layer thickness with holding temperature and time in Al/Cu ultrasonic joints [23]. Gu et al. observed interface hardening together with base-metal softening and changes in joint load during post-weld heat treatment [24]. For 0.8 mm Cu/Al sheets, Liu et al. compared interface growth during welding with predictions based on static annealing and associated the greater growth during welding with deformation-generated defects [25]. Electroplated Ni interlayers can also alter interfacial reactions and void evolution during thermal aging [26]. For a fixed Zn-assisted material system, the question addressed here is how interfacial growth relates to

the mechanical response when Al plate thickness changes and when thermal exposure continues after welding has ceased.

The present study examines this relationship in 1060 Al/T2 Cu joints containing a 0.1 mm Zn interlayer by comparing local recorded temperatures, interfacial-region dimensions, microhardness and nominal shear strength. The contribution is to establish how the association between interfacial-region growth and nominal strength changes across welding energies, plate thicknesses and subsequent thermal holding within the same material system. This comparison assesses whether a larger interfacial-region thickness consistently accompanies higher nominal strength under these different histories. Joints with 2 and 4 mm Al plates are investigated over 900–4000 J, with temperature treated as a measured response. A separate holding series uses 2 mm Al joints initially welded at 1400 J and exposed to 250 °C for 1–3 h; the no-Zn control is also restricted to 1400 J. The thickness comparison includes concurrent changes in stiffness, heat capacity and deformation. Continued interfacial growth accompanies different strength trends in these series: the 2 mm Al joints reach their highest observed mean nominal shear strength of 23.77 ± 6.70 MPa at 3000 J, the 4 mm series continues to increase to 20.50 ± 1.06 MPa at 4000 J, and the mean strength of the 1400 J joints decreases to 8.23 ± 0.83 MPa after holding for 3 h.

2. Materials and Methods

2.1. Materials, Welding and Temperature Measurement

The base materials were T2 copper (supplied by Dongguan Tongrun Copper and Aluminum Materials Co., Ltd., Dongguan, China) and 1060 aluminum plates (supplied by Zibo Yuetao Metal Materials Company, Zibo, China). Their nominal composition limits are listed in Tables 1 and 2, respectively. The Cu plates measured 13 mm × 8 mm × 1 mm. The Al plates had in-plane dimensions of 13 mm × 8 mm and thicknesses of 2 mm and 4 mm. Pure Zn foil (supplied by Hefei Shushan District Tehe Metal Materials Store, Hefei, China) with a thickness of 0.1 mm defined the fixed interlayer configuration for the energy, Al-thickness and holding comparisons. The reported experimental design does not include optimization of interlayer material or foil thickness. Before welding, the surfaces to be joined were ground with 600-grit abrasive paper, ultrasonically cleaned in ethanol (supplied by Baiyu Chemical Reagents and Glassware, Zibo, China) for 5 min, and dried. The plates were stacked with Cu above Al and the Zn foil between the two base materials.

Table 1. Specified composition limits for T2 copper (wt.%).

Cu + Ag	Bi	Sb	As	Fe	Pb	S
≥99.90	≤0.001	≤0.002	≤0.002	≤0.005	≤0.005	≤0.005

Table 2. Specified composition limits for 1060 aluminum (wt.%).

Al	Si	Fe	Cu	Mn	Mg	Zn	Ti	V
≥99.60	≤0.25	≤0.35	≤0.05	≤0.03	≤0.03	≤0.05	≤0.03	≤0.05

Ultrasonic spot welding was performed using an NC-2000P welder (Wuxi Nicle Ultrasonic Equipment Co., Ltd., Wuxi, China) with a rated maximum power of 3 kW and an operating frequency of 20 kHz. The welding horn had a 10 mm × 15 mm contact face, and the anvil measured 21 mm × 18 mm. Both surfaces were serrated, with a tooth pitch of 1 mm and a tooth depth of 0.5 mm. The equipment and joint configuration are shown in Figure 1. Welding was performed in energy-control mode, with an amplitude setting of 60% and a pressure setting of 0.2 MPa. The welding energies were 900, 1400, 2400, 3000, and 4000 J. The study focused on joints made with 2 mm Al plates, with 4 mm plates used

to assess thickness effects. Al/Cu control joints without a Zn interlayer were also produced at 1400 J. Table 3 summarizes the processing conditions for the experimental groups.

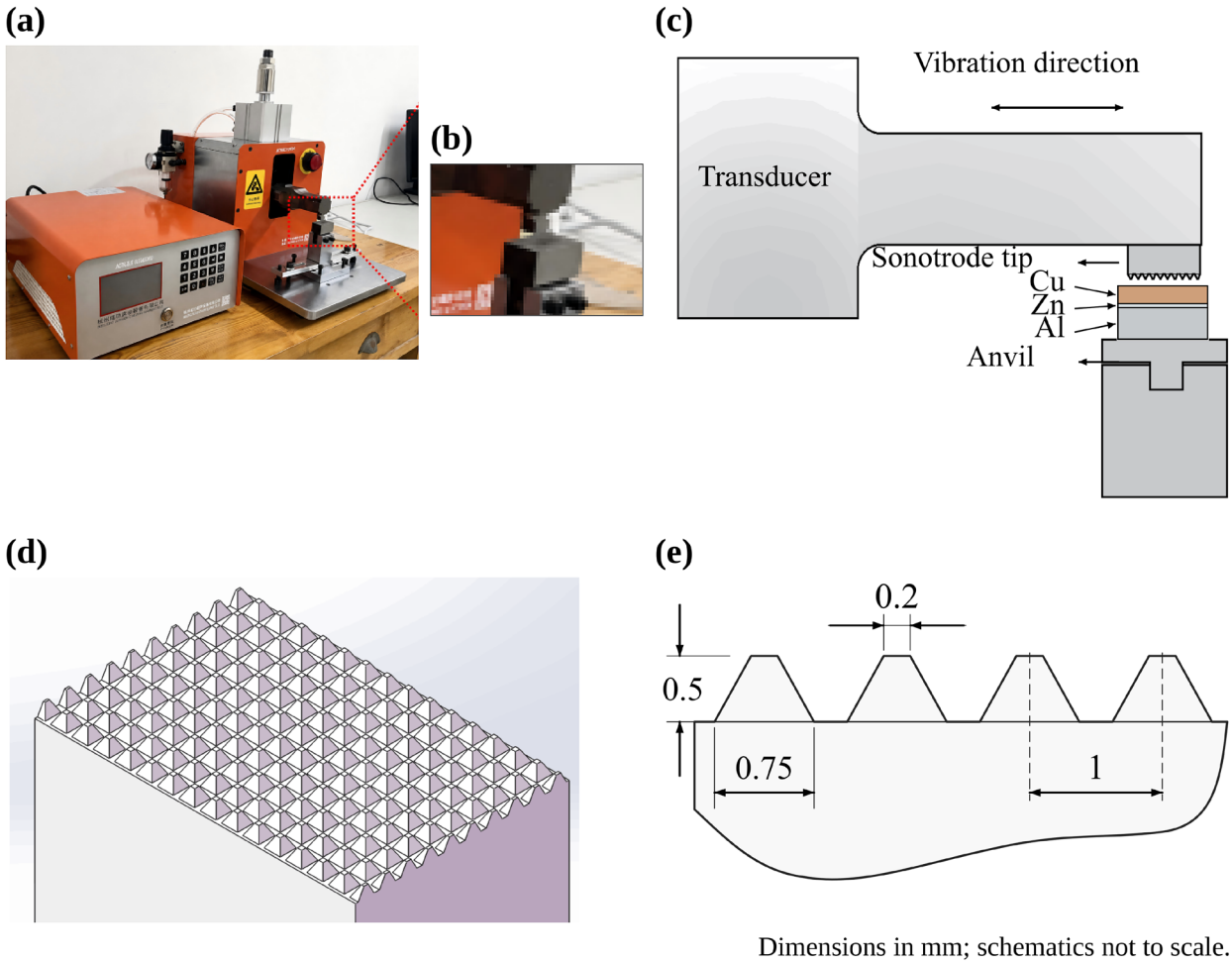

Figure 1. Ultrasonic spot-welding system and sonotrode geometry: (**a**) equipment photograph; (**b**) enlarged crop of the highlighted clamping region in (**a**); (**c**) schematic of the welding assembly and Cu/Zn/Al stack, with the vibration direction; (**d**) serrated sonotrode surface; (**e**) tooth profile and dimensions. The Chinese characters visible on the equipment are original manufacturer's labels. The equipment labels identify the ultrasonic metal welding system and include safety warnings. Dimensions in (**e**) are in mm; schematics are not to scale.

Table 3. Experimental groups and processing conditions. Three specimens were tested for nominal shear strength under each condition.

Experimental Group	Al Plate Thickness (mm)	Zn Interlayer Thickness (mm)	Welding Energy (J)	Post-Weld Condition
Zn-assisted, 2 mm Al (E2)	2	0.1	900, 1400, 2400, 3000, 4000	As-welded
Zn-assisted, 4 mm Al (E4)	4	0.1	900, 1400, 2400, 3000, 4000	As-welded
No-Zn control (C1400)	2	None	1400	As-welded
Post-weld holding (H1–H3)	2	0.1	1400	250 °C for 1, 2, or 3 h

Zn-assisted joints made with 2 mm Al plates at 1400 J were selected for post-weld heat treatment. The KF1200 box-type resistance furnace (Nanjing Boyuntong Instrument Technology Co., Ltd., Nanjing, China) was preheated to 250 °C before the specimens were

inserted. Nominal holding durations were 1, 2 and 3 h, followed by air cooling. The as-welded condition was designated 0 h. This holding series represents thermal exposure after ultrasonic welding. The 0 h reference is the 2 mm Al/1400 J condition in the energy series and is not an additional independent group.

Weld-region temperatures were measured using a K-type thermocouple (supplied by Jiangsu Hongda Measurement and Control Instrument Co., Ltd., Taizhou, China) with a wire diameter of 0.25 mm. The thermocouple was embedded in a groove on the Cu side, with its junction at the center of the weld region, and was held in place by clamping the assembled specimens (Figure 2a). Before testing, stabilized thermocouple readings were compared with those of a reference thermometer placed next to the junction in a stable indoor environment. Signals were acquired through a transmitter and a programmable logic controller (PLC, Siemens AG, Munich, Germany), then recorded in LabVIEW 2018 (National Instruments, Austin, TX, USA) at 20 Hz, corresponding to a 50 ms logging interval (Figure 2b,c). Measurements were repeated three times for each set of welding parameters. The room-temperature comparison was an operational reference check. The recording interval does not specify the sensor response time. The peaks are local recorded weld-region temperatures; a dynamic-response correction and combined measurement uncertainty are not established by the reported measurements. Junction contact, thermal inertia and heat conduction through the wire may affect the recorded maximum.

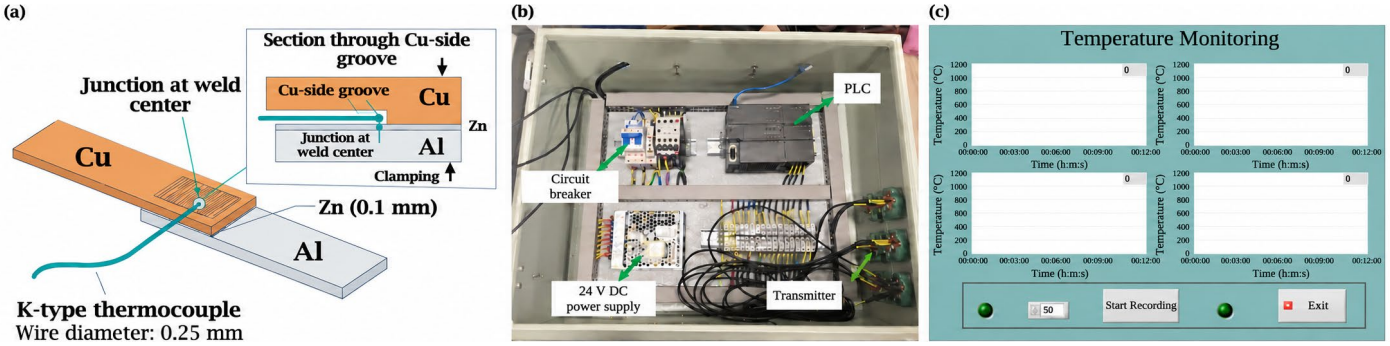

Figure 2. Weld-region temperature measurement: (**a**) schematic thermocouple installation showing the Cu-side groove, the junction at the weld-region center and fixation by specimen clamping; (**b**) photograph of the acquisition hardware with component labels; (**c**) cropped screenshot of the LabVIEW temperature-monitoring interface. The Chinese labels in panel (**c**) correspond to temperature monitoring interface, temperature channels 1–4 (°C), time (hh:mm:ss), recording, recording interval (ms), start recording, communication in progress, and exit.

2.2. Microstructural Characterization

After welding, specimens were cold-mounted, ground sequentially with 600-, 1000-, 2000- and 3000-grit abrasive papers, and polished with 2.5 μm diamond paste. Cross-sections parallel to the ultrasonic vibration direction were examined using an SDPTOP XD30M optical microscope (Ningbo Sunny Instruments Co., Ltd., Yuyao, China). Local microstructures and elemental distributions were analyzed using a Quanta 250 scanning electron microscope (SEM, FEI, Hillsboro, OR, USA) and energy-dispersive X-ray spectroscopy (EDS, EDAX, Mahwah, NJ, USA).

Image-Pro Plus 7.0 (Media Cybernetics, Rockville, MD, USA) was used to delineate each interfacial region. The Cu-side region lies between Cu and residual Zn, while the Al-side transition zone lies between residual Zn and Al. Figure 3 illustrates the Cu-side measurement within the complete joint cross-section. For each selected measurement window, A is the area enclosed by the two visible bounding interfaces and the window edges; L_1 and L_2 are the lengths of those two interfaces within the same window. Both lengths follow

the observed contours, including waviness, and exclude the transverse window edges. The mean boundary length was calculated as

$$\overline{L} = \frac{L_1 + L_2}{2}$$

The mean apparent thickness was then calculated from the delineated area and the mean boundary length:

$$\overline{t} = \frac{A}{\overline{L}} = \frac{2A}{L_1 + L_2}$$

The calculation was applied separately to the Cu-side and Al-side regions, excluding the residual Zn interlayer. The reported thicknesses describe the examined sections; specimen-level distributions and uncertainty estimates are unavailable, so small differences are interpreted descriptively.

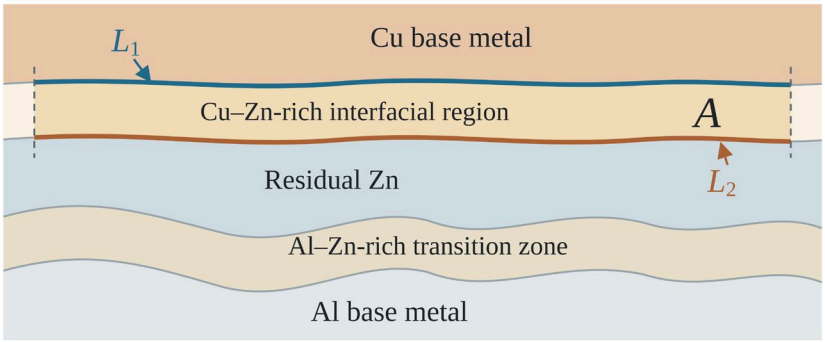

Figure 3. Area-based interfacial-thickness measurement illustrated for the Cu-side region within the complete Cu/Zn/Al cross-section. A is the delineated area, and L_1 and L_2 are the lengths of the two bounding interfaces within the same measurement window.

2.3. Microhardness and Shear Testing

Microhardness was measured along the thickness direction on polished joint cross-sections using an MH_DT1 Vickers tester (Shanghai Taiming Optical Instrument Co., Ltd., Shanghai, China) at 40× magnification, under a load of 100 gf and a dwell time of 15 s. Hardness values were calculated and output by the instrument. Figure 4 illustrates the measurement direction and material regions. For the welding-energy profiles, three specimens were measured for each condition, and values at corresponding locations were averaged. For the holding series, multiple measurements in each near-interface region of one specimen per condition were averaged. Hardness results are presented as descriptive means. At 100 gf, near-interface values are described as composite hardness because an indentation can sample an interfacial region together with adjacent constituents. These values are not assigned to the intrinsic hardness of an individual phase.

Shear-test specimens were prepared by electrical discharge machining with a nominal welded area of 4 mm × 8 mm (32 mm²). The specimen was inserted into and secured in the dedicated fixture shown in Figure 5a,b. In this configuration, the Al side was supported by the fixture and the loading member acted on the Cu side, producing relative displacement along the joint interface. Tests were performed at room temperature using an MTS Exceed universal testing machine (MTS Systems Corporation, Eden Prairie, MN, USA) at a loading rate of 1 mm/min. The maximum load F_{max} was recorded for each specimen, and the nominal shear strength was calculated as $\tau = F_{max}/S$, where $S = 32$ mm². This area is the nominal test section and does not imply complete bonding over the entire section. The reported nominal strength includes the effects of the fixture geometry and any

secondary bending; no separate correction was applied for these contributions. Both fracture surfaces were examined for local plastic deformation and interfacial failure features.

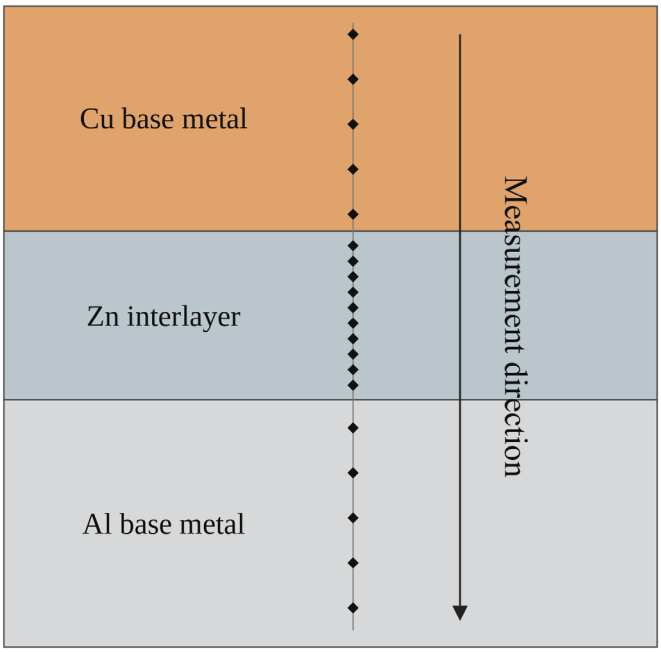

Figure 4. Schematic of microhardness measurements along the thickness direction of the Cu/Zn/Al joint. The test load and dwell time were 100 gf and 15 s, respectively. Schematic; not to scale.

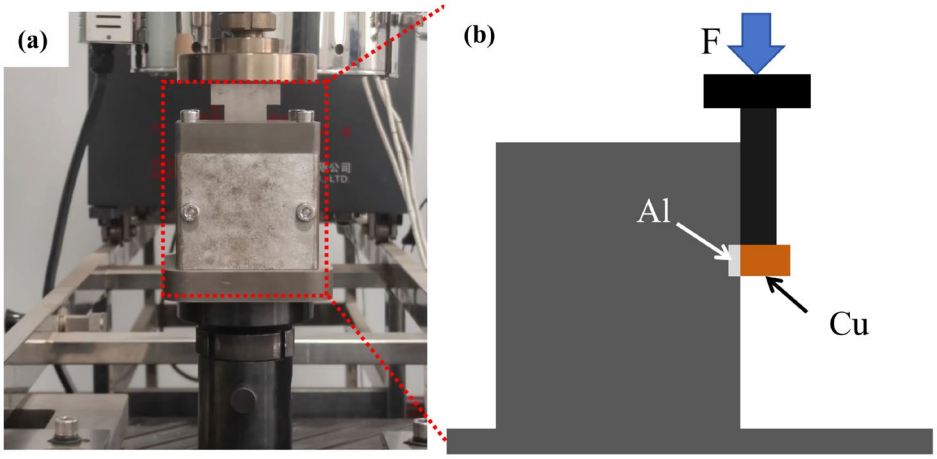

Figure 5. Shear-test arrangement: (**a**) photograph of the specimen in the dedicated fixture; (**b**) schematic of the fixture and loading direction. Panel (**b**) is not to scale.

Three specimens were tested per condition. Individual nominal shear-strength measurements, arithmetic means and sample standard deviations are presented in the Results and Discussion section. Strength plots show all three measurements and the mean ± sample SD, calculated with $n - 1$ in the denominator. The 0 h holding reference is the same as-welded 1400 J dataset used in the energy series. Comparisons and percentage changes are descriptive; statistical significance and a global optimum are not claimed for these sample sizes. Since the effective bonded-area fraction was not quantified, its contribution to nominal strength is not separated from the local strength of the bonded regions.

3. Results and Discussion

3.1. Welding Energy and Recorded Peak Weld-Region Temperature

Figure 6a compares the mean recorded peak weld-region temperatures for joints made with 2 and 4 mm Al plates. The temperature–time histories for the 2 mm Al joints at different welding energies are shown in Figure 6c. Interfacial friction and local plastic deformation provide heat while the contact state changes during welding. Li and Balle [7] resolved successive stages of relative motion in Al/Cu joints by laser Doppler vibrometry and linked the evolving system dynamics to power consumption. This connection provides a physical context for comparing temperature responses at different programmed energies. The thermocouple records describe temperatures at the sensing location; detailed heating and cooling rates, the spatial temperature field and the instantaneous maximum throughout the interface remain unresolved.

As welding energy increased from 900 to 4000 J, the mean recorded peak weld-region temperature rose from 196 to 444 °C. At 1400, 2400 and 3000 J, the mean recorded peaks were 246, 321 and 388 °C, respectively. The mean recorded peak at 4000 J was above the melting point of pure Zn, approximately 420 °C, making local Zn melting one possible contributor to interfacial evolution. The micrographs do not identify a distinct resolidified region. Thermal softening, enhanced plastic deformation and redistribution of Zn could also modify the interface at high energy.

At each programmed energy, the 4 mm Al specimens had lower thermocouple peak readings than the 2 mm specimens (Figure 6a). The mean recorded peaks for the 4 mm specimens were 180 °C at 900 J and 413 °C at 4000 J. Increasing the Al thickness changes thermal capacity as well as stiffness, vibration transmission and deformation during welding. These contributions were not separated in the present comparison. The largest recorded temperature difference between the two thicknesses was 44 °C at 3000 J. The comparison applies to the tested plate geometry, energy-control mode and machine settings.

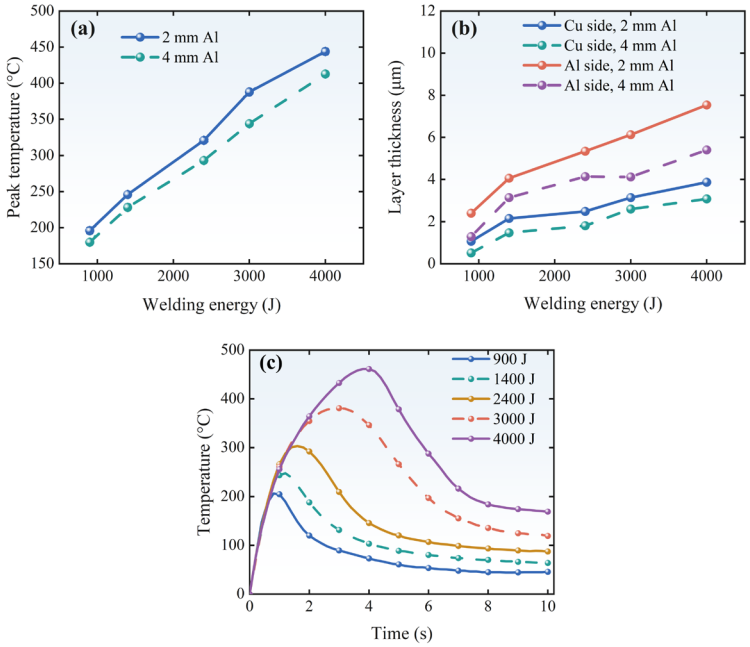

Figure 6. Effects of programmed welding energy on the interfacial response: (**a**) mean recorded peak weld-region temperatures from three measurements for each Al plate thickness and welding energy; (**b**) apparent thicknesses of the Cu-side interfacial region and Al-side transition zone for both plate thicknesses; (**c**) selected individual temperature–time histories for joints made with 2 mm Al plates at different welding energies. Panel (**a**) summarizes the recorded peak values, while panel (**c**) illustrates the heating and cooling histories of individual runs.

https://doi.org/10.3390/met16121311

3.2. Interfacial Microstructure with a Zn Interlayer

Figure 7 shows joint cross-sections at different welding energies. Al and Cu were in direct contact in joints without Zn. With a Zn interlayer, a continuous residual layer remained between the base metals, forming Cu/Zn and Zn/Al interfaces. The Cu-side interface was relatively flat, whereas the Al-side interface was locally wavy. Here, waviness describes the interface shape after welding; the foil was placed between the prepared Cu and Al mating surfaces. The groove illustrated in Figure 2 serves the separate purpose of thermocouple installation. Increasing welding energy made the Al-side waviness more pronounced and increased the apparent thickness of the Cu-side interfacial region. Local deformation under pressure and oscillatory shear, together with redistribution of Zn, offers a plausible explanation for this asymmetry. The sensitivity of contact development to the initial surface is supported by Cu-roughness experiments that related surface condition to weld-zone temperature and bonded-interface morphology [27]. Laser-pretreatment work likewise showed that cleaning and topography changes affect joint formation and process stability [28].

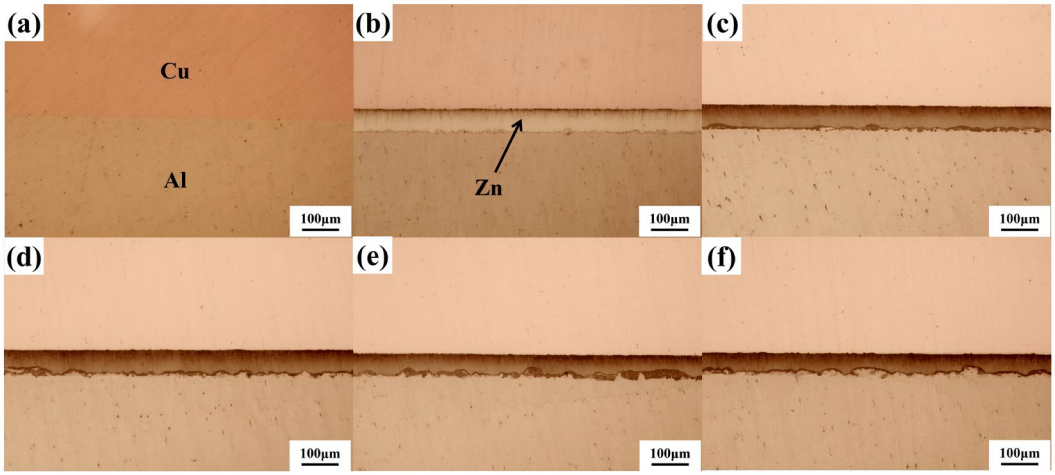

Figure 7. Optical micrographs of joint cross-sections: (**a**) joint welded at 1400 J without a Zn interlayer; (**b**–**f**) joints with a Zn interlayer welded at 900, 1400, 2400, 3000, and 4000 J, respectively.

Figure 8 compares SEM images of joints welded at 1400 J with and without a Zn interlayer. Without a Zn interlayer, unevenly distributed debris-like regions were visible near the interface, and the morphology of the bonded region varied along it. With a Zn interlayer, distinct regions appeared sequentially through the thickness. These were the Cu base metal, Cu-side interfacial region (Cu–Zn), residual Zn, Al-side transition zone (Al–Zn), and Al base metal. Table 4 lists the EDS results at representative locations. Point F, within the Cu-side interfacial region, contained 31.81 wt.% Cu and 68.19 wt.% Zn. Point G was predominantly Zn and corresponded to the residual interlayer. Point H contained 16.80 wt.% Al and 83.20 wt.% Zn, confirming the coexistence of both elements in the Al-side transition zone. The corresponding EDS line scans across the interfaces are shown in Figure 9.

The labels Cu–Zn and Al–Zn identify elemental constituents of the observed regions. SEM/EDS supports their morphology and elemental distributions; specific crystalline phases and phase fractions within the as-welded regions remain unresolved by the characterization presented here.

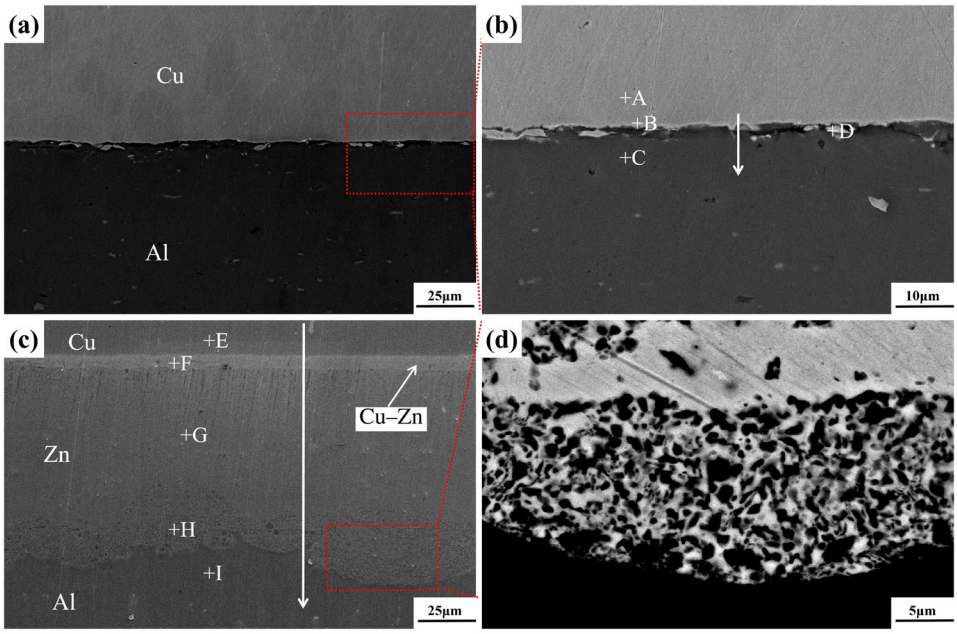

Figure 8. SEM images of joints welded at 1400 J with and without a Zn interlayer: (**a**) joint without a Zn interlayer; (**b**) enlarged view of the boxed region in (**a**); (**c**) joint with a Zn interlayer; (**d**) enlarged view of the boxed region in (**c**). The label Cu–Zn in (**c**) denotes the Cu-side interfacial region.

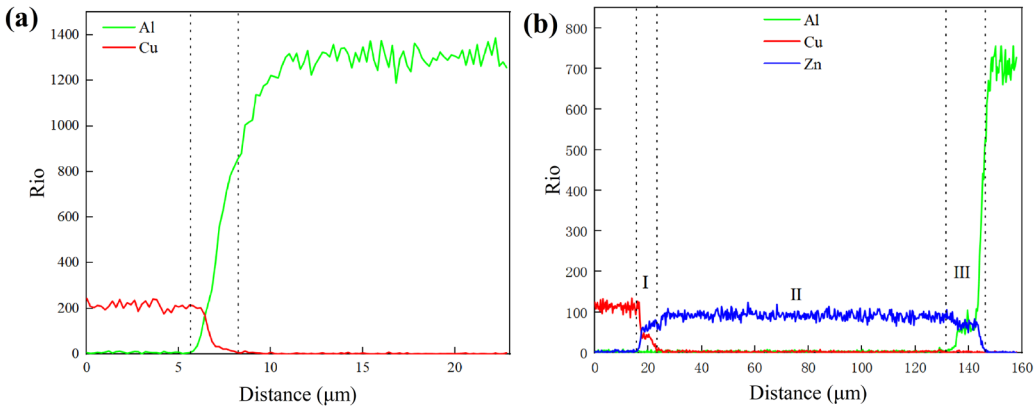

Figure 9. EDS line scans across the interfaces of joints welded at 1400 J: (**a**) joint without a Zn interlayer; (**b**) joint with a Zn interlayer.

Table 4. EDS results at representative locations in Figure 8 (wt.%).

Point	Cu	Al	Zn
A	100	—	—
B	27.13	72.87	—
C	—	100	—
D	41.36	58.64	—
E	100	—	—
F	31.81	—	68.19
G	—	—	100
H	—	16.80	83.20
I	—	100	—

Figure 6b shows that both interfacial regions thickened with increasing welding energy in joints made with 2 mm Al plates. The Cu-side interfacial region increased from 1.07 to 3.87 μm, and the Al-side transition zone increased from 2.40 to 7.54 μm. Increasing

welding energy from 3000 to 4000 J increased the reported dimensions by 0.73 and 1.41 μm, respectively. These values describe the observed interfacial regions, whose widths and morphologies varied locally; they are not thicknesses of independently identified single phases.

3.3. Microhardness and Shear Properties

Figure 10 shows the reported microhardness profiles through the joint thickness. The Cu base metal mainly exhibited hardness values of 70–95 HV0.1, compared with approximately 30–40 HV0.1 in Al and 40–50 HV0.1 in the Zn-containing region. The base-metal values decreased slightly with increasing welding energy, while the Zn-containing and near-interface values increased to varying degrees. These contrasting local responses call for consideration of the material sampled at each location. In Al/Cu ultrasonic torsional joints, Zhao et al. [29] evaluated local hardness together with surface morphology when examining interfacial integrity. Here, thermal exposure may contribute to base-metal softening, while compressive deformation and local microstructural evolution can affect the Zn-containing region. At 100 gf, the near-interface measurements represent a composite indentation response whose value depends on the dimensions and proportions of the constituents sampled.

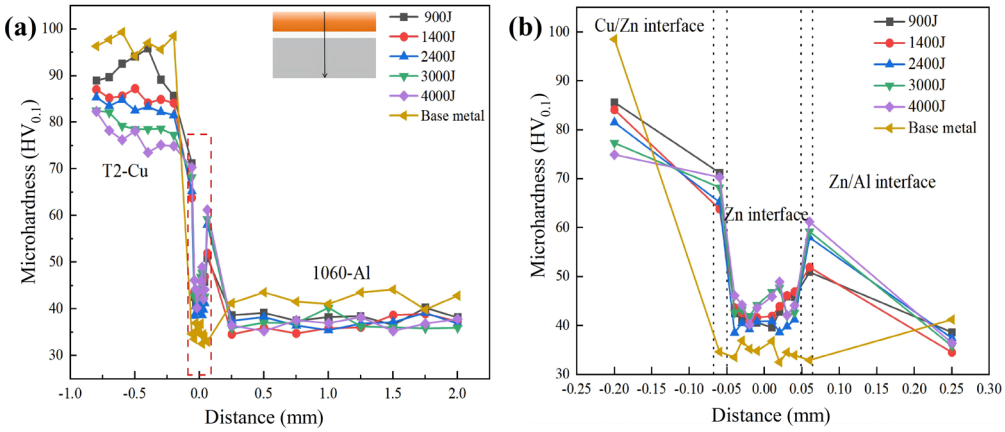

Figure 10. Microhardness profiles of joints produced at different welding energies: (**a**) full profiles; (**b**) enlarged view. Points represent means at corresponding measurement positions in three specimens. Near-interface values describe composite indentation responses under a 100 gf load.

For joints made with 2 mm Al plates, the mean nominal shear strengths at 900, 1400, 2400, 3000 and 4000 J were 9.76 ± 4.88, 11.97 ± 7.02, 18.21 ± 4.74, 23.77 ± 6.70 and 18.85 ± 2.47 MPa, respectively (mean ± sample SD, n = 3; Figure 11a). The mean at 4000 J was 20.7% below that at 3000 J. Individual measurements show substantial scatter, particularly at 1400 and 3000 J. Accordingly, 3000 J is described as the condition with the highest observed mean among the tested energies, without a claim of a statistically established optimum. Between 3000 and 4000 J, both interfacial regions continued to grow while the mean nominal strength decreased.

Development of connected regions and deformation of the surrounding sheet can both influence the energy response. Work on multilayer Cu–Al foil stacks associated weld quality with microbond development, material flow and interface morphology [30]. Ma et al. [9] further described repeated formation and breakage of micro-welds during Al/Cu welding, followed by greater interfacial contact as deformation progressed. Such observations identify bonded area and local sheet geometry as relevant quantities when interpreting the highest mean measured at 3000 J in the present 2 mm series. The available energy-series data do not quantify bonded area, indentation depth or remaining sheet

thickness. Fracture observations are confined to the 1400 J Zn/no-Zn comparison, and the mechanical dataset provides maximum loads without an analysis of load–displacement behavior.

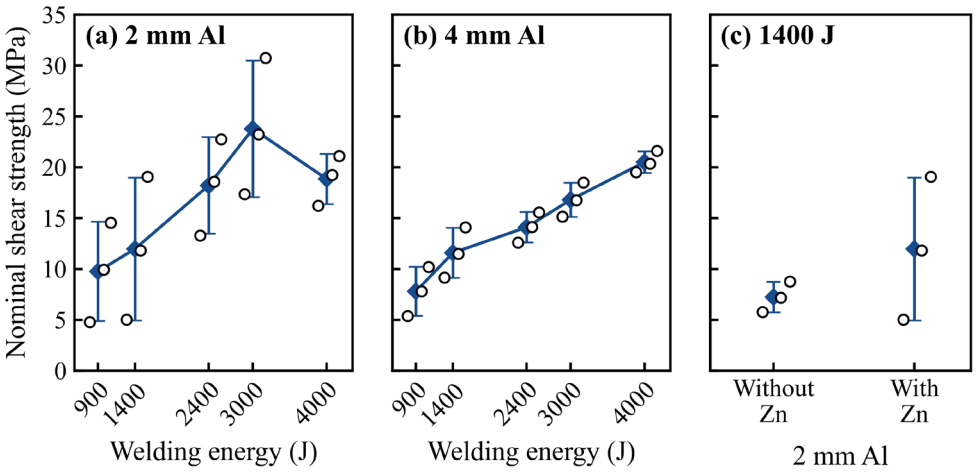

Figure 11. Nominal shear strength: (**a**) Zn-assisted joints with 2 mm Al plates at different welding energies; (**b**) Zn-assisted joints with 4 mm Al plates; (**c**) joints with and without a Zn interlayer at 1400 J using 2 mm Al plates. Open circles show individual specimens; diamonds and error bars show arithmetic means ± one sample standard deviation (n = 3). All panels use the same strength scale. The Zn-assisted 1400 J data in (**a**) and (**c**) are the same measurements.

At 1400 J, the 2 mm Al joints had mean nominal shear strengths of 7.23 ± 1.50 MPa without Zn and 11.97 ± 7.02 MPa with Zn (n = 3; Figure 11c). The difference between the observed means was 4.74 MPa, or 65.6%. This comparison used the same programmed energy, amplitude setting and pressure setting. Adding Zn changes contact, friction, deformation and potentially the thermal history, so equal programmed energy does not establish equal interfacial energy absorption. A continuous residual Zn layer remained under this condition. Trial welding without Zn at 2400 J caused Al plate deformation and sticking to the anvil; the quantitative Zn/no-Zn comparison was therefore restricted to 1400 J. The result does not establish a general strengthening benefit across welding energies or a comparison between independently optimized processes.

3.4. Post-Test Separation Surface Morphology

Figure 12 shows the surfaces exposed after shear-test separation of the joint welded at 1400 J without Zn. Panels (a) and (c) are low-magnification views of the Cu-side and Al-side specimens, respectively; panels (b) and (d) show selected higher-magnification views from the corresponding sides. The EDS compositions, expressed as mass fractions normalized to the listed elements, are given in Table 5. The Cu-side surface contained relatively flat areas and patches of adherent material, while local deformation features were visible at higher magnification and on the Al-side surface. These observations describe the exposed surfaces after testing; low-magnification flat areas alone do not distinguish all pre-existing unbonded areas from regions created during separation or establish a uniform fracture mode.

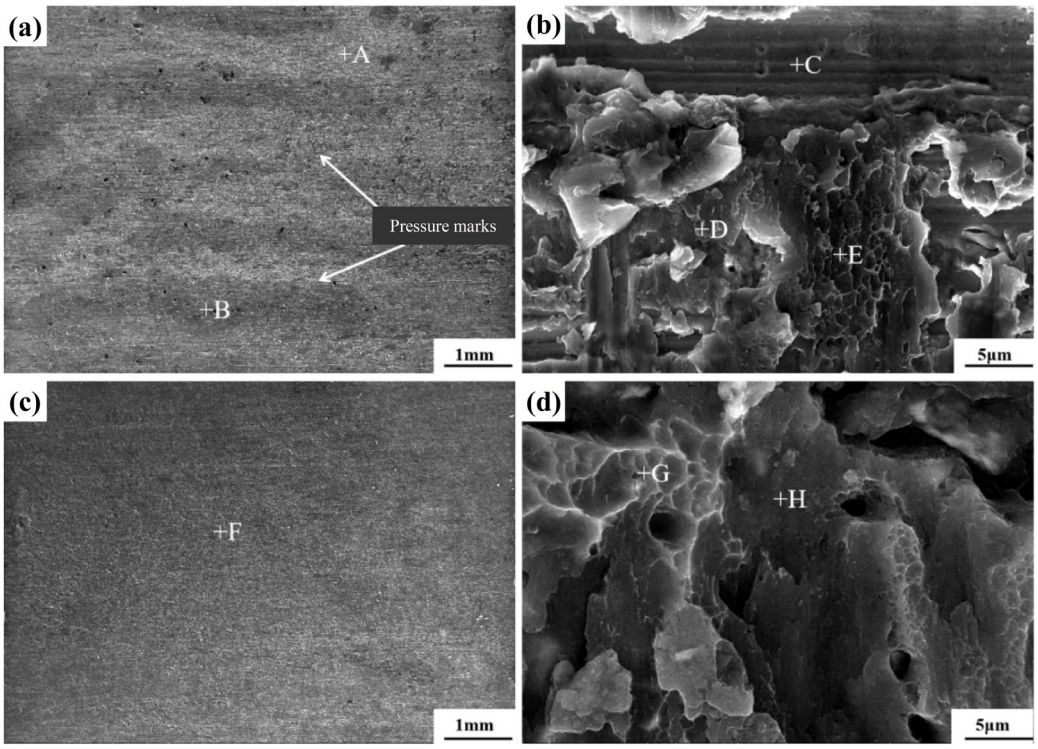

Figure 12. SEM images of surfaces exposed after shear-test separation of as-welded joints produced at 1400 J without Zn: (**a**) Cu-side view; (**b**) higher-magnification Cu-side view; (**c**) Al-side view; (**d**) higher-magnification Al-side view.

Table 5. EDS compositions (wt.%, normalized to the listed elements) of the fracture surfaces of the joint welded at 1400 J without a Zn interlayer.

Point	Cu (wt.%)	Al (wt.%)
A	32.47	67.53
B	80.35	19.65
C	85.09	14.91
D	20.85	79.15
E	47.29	52.71
F	23.85	76.15
G	14.05	85.95
H	15.17	84.83

Residual material was observed on both fracture surfaces of the joint with a Zn interlayer (Figure 13). Banded rubbing marks were also present on the Al-side fracture surface. The corresponding EDS mass fractions, normalized to the listed elements, are given in Table 6. Compared with the joint without a Zn interlayer, the Cu-side fracture surface showed more pronounced dimples while retaining many flat fracture regions. Load transfer depends on the extent of connected regions and the deformation concentrated around their boundaries. Arweiler-Böllert et al. [8] examined this relationship through interface-geometry characterization and models of local damage, linking both aspects to the overall tensile-shear response. The surface-configuration study by Abbas et al. [31] also showed that a more consistent failure location could accompany a lower peak load. The effective bonded-area fraction and intrinsic interfacial resistance remain unquantified in the present comparison. At 1400 J, the observed dimples and rubbing marks provide evidence of local deformation during separation.

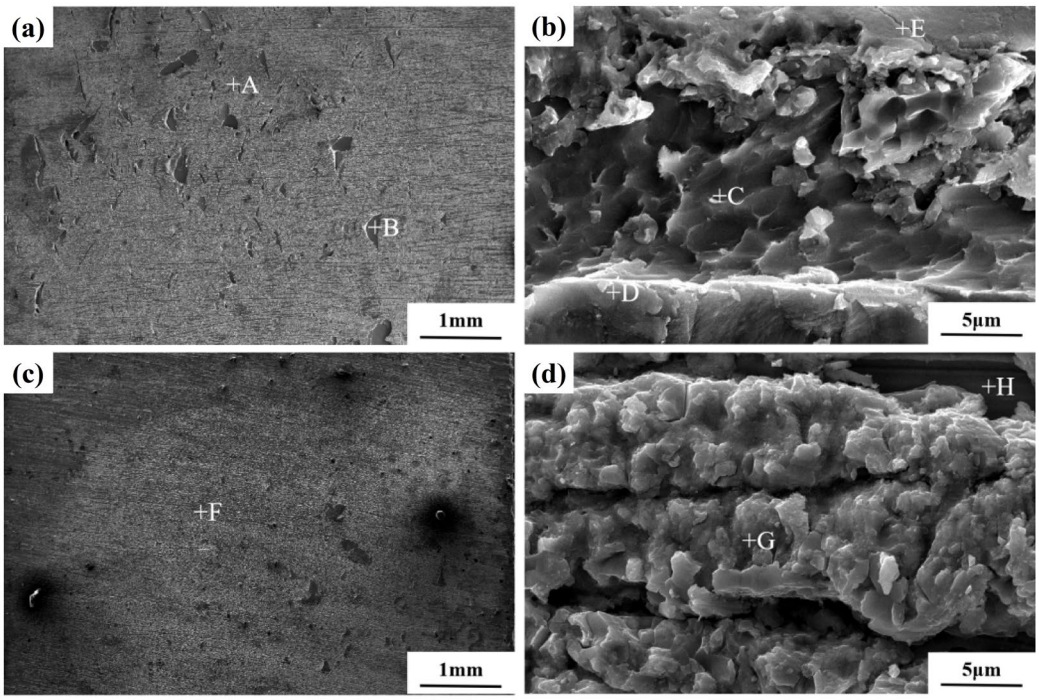

Figure 13. SEM images of surfaces exposed after shear-test separation of as-welded joints produced at 1400 J with Zn: (**a**) Cu-side view; (**b**) higher-magnification Cu-side view; (**c**) Al-side view; (**d**) higher-magnification Al-side view.

Table 6. EDS compositions (wt.%, normalized to the listed elements) of the fracture surfaces of the joint welded at 1400 J with a Zn interlayer.

Point	Cu (wt.%)	Al (wt.%)	Zn (wt.%)
A	21.99	—	78.01
B	83.22	—	16.78
C	1.88	—	98.12
D	6.55	—	93.45
E	10.85	—	89.15
F	—	0.16	99.84
G	—	12.88	87.12
H	—	43.36	56.64

3.5. Effect of Al Plate Thickness on the Welding Response

Increasing the Al plate thickness from 2 to 4 mm preserved the overall interface morphology, with a relatively straight Cu-side interface and a locally wavy Al-side interface (Figure 14). For the 4 mm Al joints, the reported apparent thickness of the Cu-side interfacial region increased from 0.52 to 3.08 μm over 900–4000 J. At each tested energy, this region was thinner than in the 2 mm Al joints, and the recorded peak weld-region temperature was lower. The corresponding Al-side transition-zone values were 1.29, 3.14, 4.14, 4.12 and 5.41 μm (Figure 6b). Figure 14b–f identify the region locations and label these reported apparent thickness estimates. The values at 2400 and 3000 J were similar, at 4.14 and 4.12 μm. At 900 J, local unbonded regions remained visible in the examined cross-section. These thickness values describe the analyzed sections and do not resolve variation between specimens.

The visible unbonded regions can reduce the area available to carry load. A cross-section does not provide the bonded-area fraction of the entire interface, so the nominal-

strength comparison retains the combined influence of bonded area and local interfacial strength.

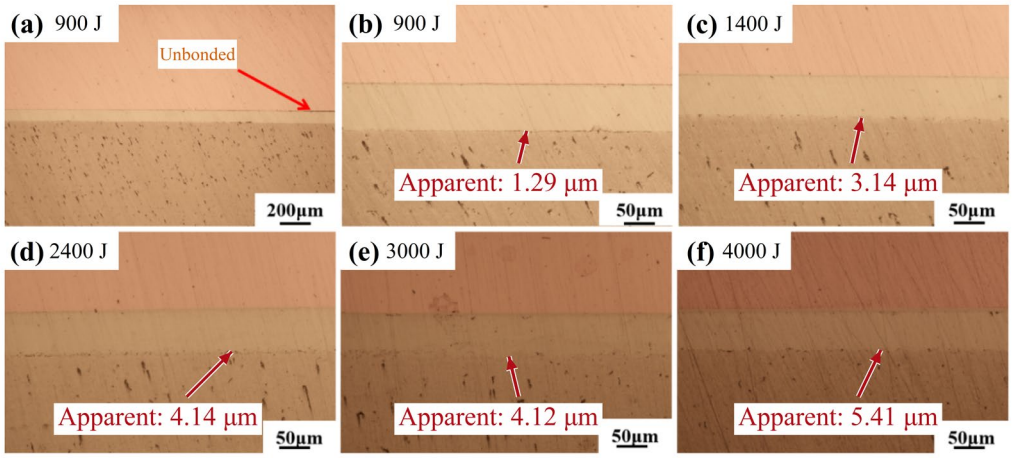

Figure 14. Optical micrographs of cross-sections of Zn-assisted joints made with 4 mm Al plates: (**a**,**b**) 900 J; (**c**) 1400 J; (**d**) 2400 J; (**e**) 3000 J; (**f**) 4000 J. Arrows in (**b**–**f**) identify the Al-side transition region. Numerical labels give the reported apparent thickness estimate for each condition; the arrows indicate region locations and do not measure local thickness.

With the amplitude setting held at 60% and the pressure setting at 0.2 MPa, mean nominal shear strength for the 4 mm Al specimens increased from 7.80 ± 2.40 MPa at 900 J to 11.58 ± 2.47, 14.10 ± 1.49, 16.80 ± 1.67 and 20.50 ± 1.06 MPa at 1400, 2400, 3000 and 4000 J, respectively (n = 3; Figure 11b). This increasing trend occurred together with lower recorded temperatures and thinner interfacial regions than in the 2 mm series. A change in thickness also changes the dynamic response of the workpiece: Müller et al. [16] linked geometry and natural frequencies to vibration transmission, power consumption and bond strength. The different heat generation and peel loads reported for layer-wise and stacked joints [17] similarly illustrate how the specimen arrangement affects the welding response. In the present 13 mm × 8 mm plate geometry, thermal capacity, stiffness and deformation change concurrently, and their individual contributions were not determined. The 4 mm series ended at 4000 J, where its highest observed mean occurred.

3.6. Effects of Post-Weld Holding at 250 °C

After post-weld holding at 250 °C, the joints welded at 1400 J retained the overall contours of both interfaces (Figure 15). The interfacial regions thickened, and the residual Zn layer diminished. The apparent thickness of the Cu-side interfacial region increased from 2.15 μm in the as-welded condition to 19.13 μm after 1 h and 46.12 μm after 3 h. The Al-side transition zone thickened from 4.06 to 36.12 μm after 3 h (Figure 16a). Compared with the brief temperature rise during ultrasonic spot welding, isothermal post-weld holding provided more time for diffusion and reaction, which is consistent with continued growth of the interfacial regions.

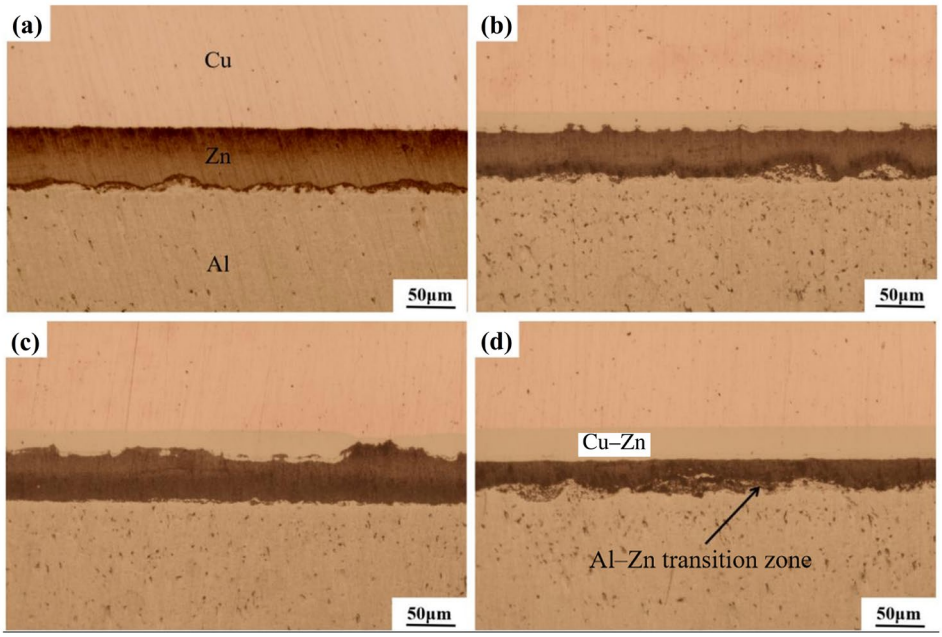

Figure 15. Cross-sectional microstructures of joints welded at 1400 J and held at 250 °C for different durations: (**a**) 0 h; (**b**) 1 h; (**c**) 2 h; (**d**) 3 h. The label Cu–Zn in (**d**) denotes the Cu-side interfacial region.

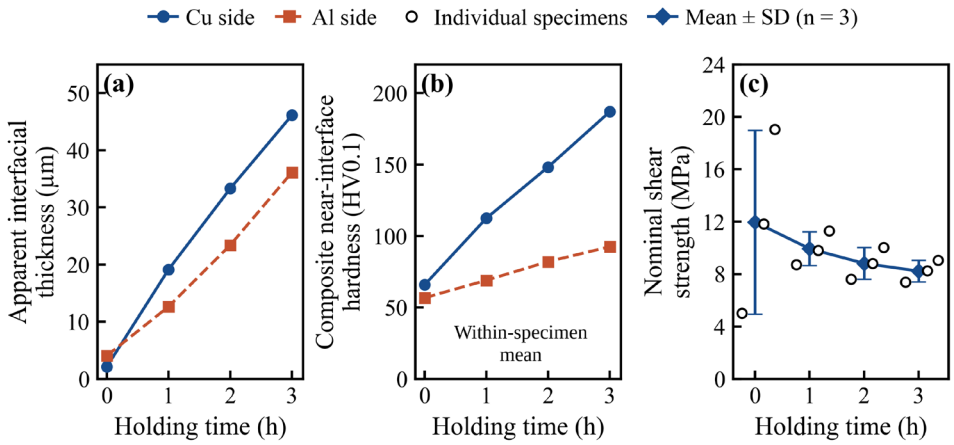

Figure 16. Effects of holding time at 250 °C on joints welded at 1400 J using 2 mm Al plates: (**a**) apparent thicknesses of the Cu-side interfacial region and Al-side transition zone; (**b**) mean composite near-interface hardness, calculated from multiple measurements within each side of one specimen per condition; (**c**) individual nominal shear strengths and arithmetic means ± one sample standard deviation (n = 3 specimens).

The mean composite near-interface hardness increased with holding time on both sides. The Cu-side value rose from 65.90 to 186.93 HV0.1, while the Al-side value increased from 56.80 to 92.48 HV0.1 (Figure 16b); each reported value is the mean of multiple measurements within the corresponding region of one specimen. As the interfacial regions thickened and residual Zn diminished, the relative amounts of the constituents sampled by an indentation could also change. The measured increase consequently describes the combined near-interface response under a 100 gf load, with a larger increase on the Cu side. It does not establish an intrinsic phase hardness or demonstrate that hardening alone caused the accompanying change in nominal shear strength.

Holding times of 0, 1, 2 and 3 h at 250 °C corresponded to mean nominal shear strengths of 11.97 ± 7.02, 9.94 ± 1.29, 8.82 ± 1.21 and 8.23 ± 0.83 MPa, respectively (n = 3; Figure 16c). The mean after 3 h was 31.2% below the as-welded mean. These percentages describe the measured sample means. The lower means developed concurrently with interfacial growth and increasing composite near-interface hardness. Thermal-processing experiments on Al/Cu joints by Ao et al. [23] likewise linked longer or hotter exposure to interfacial growth and changes in load-bearing capacity. Gu et al. [24] examined hardness and bond development alongside the joint load, showing that interface hardening can coexist with base-metal softening.

The relationship between interfacial growth and nominal strength differed between welding and post-weld holding. For the 2 mm Al joints, growth of both interfacial regions accompanied an increase in mean strength from 900 to 3000 J. During holding of the 1400 J joints, the regions continued to grow while mean strength decreased. Welding combines reciprocating shear with evolving contact and deformation, while holding extends thermal exposure after vibration has ceased. Liu et al. [25] found that static-annealing growth constants underpredicted the interface growth observed during Cu/Al ultrasonic welding and associated the difference with deformation-generated defects. At the atomic scale, simulations of Cu/Al bicrystals showed that shear and grain-boundary sliding promote interfacial rearrangement, with grain boundaries also facilitating diffusion [32]. These observations support the idea of considering the mechanical and thermal histories together when comparing the two stages. Void or crack formation and changes in fracture path across holding times remain unestablished in the present series. Reduction of the residual Zn layer could change deformation accommodation, and base-metal softening may also contribute to the mechanical response.

The thickness and holding comparisons show that interfacial-region growth is associated with different nominal-strength responses within the same material system. The 2 mm specimens had their highest measured mean at 3000 J, whereas the 4 mm specimens continued to gain mean strength up to 4000 J. The separate holding series underwent further interfacial growth together with a lower mean strength. Because thermal histories and effective bonded areas were not matched across these comparisons, the data do not define a universal critical interfacial thickness.

Table 7 places the present results alongside selected Al/Cu ultrasonic joints using the force or strength metric reported in each study. The present 3000 J result of 23.77 ± 6.70 MPa corresponds to a mean maximum load of 760.64 ± 214.46 N. After 250 °C holding for 3 h, the 1400 J joints carried 263.36 ± 26.50 N, corresponding to 8.23 ± 0.83 MPa (mean ± sample SD, n = 3). In Zn-free joints, Gu et al. [24] reported loads of 2.458 kN after 200 °C for 1 h and 3.138 kN after 500 °C for 1 h. The material and test details listed with these values make the differences in alloys, specimen geometry, area definition, loading arrangement and thermal history explicit. The comparison concerns performance under those respective conditions. Figures 11 and 16c show the individual nominal shear-strength measurements and sample variability for the present configuration.

Table 7. Selected reported mechanical results for Al/Cu ultrasonic joints and the present study. The materials, processing conditions and original force or strength units are retained.

Study	Materials and Geometry	Welding and Thermal Conditions	Mechanical Result
Li et al. [19]	Al/Cu with Zn; Al and Cu each 0.5 mm thick. Figure 2 of Ref. [19] shows 25 mm width, 25 mm overlap and an 8 × 8 mm weld region.	700 J; as-welded.	Approximately 1450 N with Zn, read from Figure 9 of Ref. [19] (bearing load capacity F, in N).

Li et al. [3]	EN AW 1050 Al / EN CW 008A Cu, both 1 mm; 70 × 15 mm specimens; 15 × 15 mm overlap; 10 × 10 mm sonotrode.	20 kHz; 28 μm amplitude; 700 N force; welding durations of 75–700 ms; as-welded.	Mean tensile-shear failure-load plateau of 1663–1820 N after approximately 400 ms.
Gu et al. [24]	6082-T6 Al / T2 Cu, both 1 mm; 25 × 25 mm plates; no Zn interlayer.	20.11 kHz; 1400 J; 9.5 μm amplitude; 0.4 MPa. Post-weld holding for 1 h.	2.458 kN after 200 °C holding; 3.138 kN after 500 °C holding.
Present study: selected 2 mm Al conditions	1060 Al (2 mm) / Zn (0.1 mm) / T2 Cu (1 mm); 13 × 8 mm plates; nominal shear-test area 32 mm^2.	20 kHz; 60% amplitude setting; 0.2 MPa. (i) 3000 J, as-welded; (ii) 1400 J followed by 250 °C for 3 h.	(i) 760.64 ± 214.46 N; 23.77 ± 6.70 MPa. (ii) 263.36 ± 26.50 N; 8.23 ± 0.83 MPa. Means ± sample SD, n = 3.

Electrical resistance and temperature rise under current loading were not measured. The results address interfacial morphology and room-temperature nominal shear performance of the tested plate joints; suitability for battery-tab or busbar service remains unverified.

4. Conclusions

(1) Ultrasonic spot welding joined 1060 Al and T2 Cu using a 0.1 mm Zn interlayer. The joints contained a relatively straight Cu–Zn-rich interfacial region and a wavy Al–Zn-rich transition zone. For 2 mm Al specimens, the mean recorded peak temperature increased from 196 to 444 °C over 900–4000 J, and both interfacial regions thickened. The highest observed mean nominal shear strength among the tested energies was 23.77 ± 6.70 MPa at 3000 J; the mean at 4000 J was 18.85 ± 2.47 MPa (n = 3).

(2) At the tested 1400 J setting for 2 mm Al specimens, mean nominal shear strength was 11.97 ± 7.02 MPa with Zn and 7.23 ± 1.50 MPa without Zn (n = 3), corresponding to a 65.6% difference between the means. The Zn-assisted joint showed more pronounced local dimples on the Cu-side fracture surface. The comparison is confined to this programmed energy and specimen configuration.

(3) Under the same programmed energy, amplitude setting and pressure setting, the tested 4 mm Al specimens showed lower recorded peak temperatures and thinner interfacial regions than the 2 mm specimens. Their mean nominal shear strength increased over 900–4000 J and reached 20.50 ± 1.06 MPa at the upper tested energy of 4000 J (n = 3). The thickness comparison includes concurrent changes in specimen stiffness, thermal capacity and deformation.

(4) Holding the 2 mm Al joints welded at 1400 J at 250 °C for 3 h increased the reported Cu-side and Al-side region thicknesses to 46.12 and 36.12 μm, respectively. Composite near-interface hardness increased, while mean nominal shear strength was 8.23 ± 0.83 MPa (n = 3 shear-test specimens), 31.2% below the as-welded mean. Interfacial growth, residual-Zn depletion and the change in nominal strength occurred concurrently; their individual contributions to failure were not separated.

Author Contributions: Conceptualization, T.Q. and M.N.O.Z.; methodology, T.Q. and Q.C.; formal analysis, T.Q., Q.Y. and D.L.; investigation, T.Q. and Q.C.; data curation, T.Q.; writing—original draft preparation, T.Q.; writing—review and editing, Q.Y., M.N.O.Z., D.L. and Q.C.; visualization, T.Q.; supervision, M.N.O.Z. All authors have read and agreed to the published version of the manuscript.

Funding: This research was supported by the Intelligent Manufacturing Engineering Laboratory of Shandong Huayu University of Technology (PT2025KJS002).

Data Availability Statement: The original contributions presented in this study are included in the article. Further inquiries can be directed to the corresponding author.

Conflicts of Interest: The authors declare no conflicts of interest.

References

1. de Leon, M.; Shin, H.S. Prediction of Optimum Welding Parameters for Weld-Quality Characterization in Dissimilar Ultrasonic-Welded Al-to-Cu Tabs for Li-ion Batteries. *Met. Mater. Int.* **2023**, *29*, 1079–1094. https://doi.org/10.1007/s12540-022-01271-z.
2. Sharma, V.; Manna, I.; Das, A. Evaluation of multi-layered Al foils to Cu tab ultrasonic welds for Li-ion battery applications. *Mater. Manuf. Processes* **2025**, *40*, 2142–2151. https://doi.org/10.1080/10426914.2025.2575176.
3. Li, J.; Zillner, J.; Balle, F. In-Depth Evaluation of Ultrasonically Welded Al/Cu Joint: Plastic Deformation, Microstructural Evolution, and Correlation with Mechanical Properties. *Materials* **2023**, *16*, 3033. https://doi.org/10.3390/ma16083033.
4. Liu, J.; Cao, B.; Yang, J. Texture and intermetallic compounds of the Cu/Al dissimilar joints by high power ultrasonic welding. *J. Manuf. Processes* **2022**, *76*, 34–45. https://doi.org/10.1016/j.jmapro.2022.02.001.
5. Yusefi, A.; Kokabi, A.H.; Abedini, R.; Fartashvand, V.; Allahverdizadeh, V. Microstructure evolution and mechanical properties analysis in dissimilar ultrasonic metal welding of aluminum to copper. *J. Mater. Res. Technol.* **2024**, *30*, 2922–2935. https://doi.org/10.1016/j.jmrt.2024.04.037.
6. Goodarzi, N.; Hashemi, R.; Abedini, R. Microstructure investigation and optimization of process parameters of ultrasonic welding for Al–Cu dissimilar joints using design of experiment. *J. Mater. Res. Technol.* **2024**, *31*, 2236–2248. https://doi.org/10.1016/j.jmrt.2024.06.198.
7. Li, J.; Balle, F. In-situ observation of the bond formation process during ultrasonic metal welding of Al/Cu joints using Laser Doppler Vibrometry. *J. Manuf. Processes* **2023**, *106*, 1–11. https://doi.org/10.1016/j.jmapro.2023.09.077.
8. Arweiler-Böllert, S.; Liesegang, M.; Beck, T.; Jungbluth, J.; Schmeer, S. Relation Between Interface Geometry and Tensile Shear Strength of Ultrasonically Welded Joints. *J. Mater. Eng. Perform.* **2023**, *32*, 10469–10485. https://doi.org/10.1007/s11665-023-08325-2.
9. Ma, Q.; Song, C.; Zhou, J.; Zhang, L.; Ji, H. Dynamic Weld evolution during ultrasonic welding of Cu–Al joints. *Mater. Sci. Eng. A* **2021**, *823*, 141724. https://doi.org/10.1016/j.msea.2021.141724.
10. Zhang, Z.; Wang, K.; Li, J.; Yu, Q.; Cai, W. Investigation of Interfacial Layer for Ultrasonic Spot Welded Aluminum to Copper Joints. *Sci. Rep.* **2017**, *7*, 12505. https://doi.org/10.1038/s41598-017-12164-2.
11. Go, B.S.; Kim, K.H.; Ro, C.S.; Bang, H.S. Influence of Process Parameters on Formation of Al/Cu Dissimilar Weld Using Ultrasonic Welding. *Int. J. Precis. Eng. Manuf.* **2022**, *23*, 1359–1365. https://doi.org/10.1007/s12541-022-00651-0. Correction in *Int. J. Precis. Eng. Manuf.* **2023**, *24*, 143. https://doi.org/10.1007/s12541-022-00748-6.
12. Yusefi, A.; Kokabi, A.H.; Abedini, R.; Fartashvand, V.; Allahverdizadeh, V. Investigation of Process Parameters on the Mechanical Strength in Ultrasonic Metal Welding of Aluminum to Copper Dissimilar Joints. *Trans. Indian Inst. Met.* **2024**, *77*, 3707–3718. https://doi.org/10.1007/s12666-024-03443-4.
13. Tokita, S.; Liu, C.Y.; Sato, Y.S. Effects of material combination for ultrasonic spot welding on microstructure and strength of Al/Al, Al/Cu, and Al/Ni dissimilar joints. *J. Mater. Res. Technol.* **2023**, *26*, 7619–7633. https://doi.org/10.1016/j.jmrt.2023.09.094.
14. Xu, Z.; Zhang, Y. Improvement on microstructure and mechanical properties of Cu/Al ultrasonic spot welded joints assisted by periodic additional force. *J. Mater. Process. Technol.* **2024**, *326*, 118325. https://doi.org/10.1016/j.jmatprotec.2024.118325.
15. Zhao, L.; Abbas, Z.; Su, J.; Li, L.; Li, M. Effect of thickness variation on ultrasonic welding of aluminum-copper joints. *Proc. Inst. Mech. Eng. Part L J. Mater. Des. Appl.* **2026**, *240*, 788–798. https://doi.org/10.1177/14644207251352308.
16. Müller, F.W.; Liu, J.; Schiebahn, A.; Reisgen, U. Influence of workpiece geometry and natural frequencies on ultrasonic metal welding. *Proc. Inst. Mech. Eng. Part L J. Mater. Des. Appl.* **2024**, *238*, 2343–2375. https://doi.org/10.1177/14644207241245431.
17. Sharma, V.; Das, A. A Comparison of Multi-Layered Ultrasonic Joints Fabrication using Layer-Wise vs Stacked Approaches for Battery Interconnects. *Manuf. Lett.* **2025**, *43*, 75–78. https://doi.org/10.1016/j.mfglet.2025.01.003.
18. Balasundaram, R.; Patel, V.K.; Bhole, S.D.; Chen, D.L. Effect of zinc interlayer on ultrasonic spot welded aluminum-to-copper joints. *Mater. Sci. Eng. A* **2014**, *607*, 277–286. https://doi.org/10.1016/j.msea.2014.03.135.
19. Li, C.; Ao, S.; Wang, A.; Wei, Q.; Wu, M.; Luo, Z. Mechanical Behavior and Microstructure of Ultrasonic-Spot-Welded Al/Cu Dissimilar Joints with Zn Interlayer. *Trans. Tianjin Univ.* **2020**, *26*, 305–313. https://doi.org/10.1007/s12209-019-00221-y.

20. Deng, J.; Abbas, Z.; Zhao, L.; Tang, Z.; Chen, W.; Gong, T. Forming Quality and Failure Behaviors of Al/Cu Ultrasonic Welding Joints with Additional Ni, Zn, and Mg Interlayers. *J. Mater. Eng. Perform.* **2025**, *34*, 9516–9532. https://doi.org/10.1007/s11665-024-09774-z.
21. Das, S.; Mahanta, T.; Satpathy, M.P.; Pattanayak, S. Strengthening Al-Cu ultrasonic spot welds using Ni interlayer for superior joint performance. *Mater. Manuf. Processes* **2025**, *40*, 1133–1142. https://doi.org/10.1080/10426914.2025.2476445.
22. Gan, G.; Li, F.; Geng, M.; Zhang, J.; Du, Y.; Yang, D.; Pan, H. Low-temperature Cu/Al solid-state bonding with SAC307 + Zn composite interlayer: Achieving robust long-term isothermal aging reliability via ultrasonic-assistance. *J. Mater. Sci. Mater. Electron.* **2026**, *37*, 1425. https://doi.org/10.1007/s10854-026-17839-z.
23. Ao, S.; Li, C.; Zhang, W.; Wu, M.; Dai, Y.; Chen, Y.; Luo, Z. Microstructure evolution and mechanical properties of Al/Cu ultrasonic spot welded joints during thermal processing. *J. Manuf. Processes* **2019**, *41*, 307–314. https://doi.org/10.1016/j.jmapro.2019.04.006.
24. Gu, X.; Liu, D.; Liu, J. Effect of Post-weld Heat Treatment on the Dissimilar Cu/Al Joints Produced by High Power Ultrasonic Spot Welding. *ISIJ Int.* **2018**, *58*, 1721–1726. https://doi.org/10.2355/isijinternational.ISIJINT-2017-694.
25. Liu, J.; Cao, B.; Yang, J. Effects of Vibration Amplitude on Microstructure Evolution and Mechanical Strength of Ultrasonic Spot Welded Cu/Al Joints. *Metals* **2017**, *7*, 471. https://doi.org/10.3390/met7110471.
26. Jeong, J.M.; Kim, D.; Kim, J.; Bang, J.; Jung, S.B.; Kim, M.S. Improving mechanical stability of Al/Cu ultrasonic bonded joint for battery tab by adopting electroplated Ni interlayer. *J. Mater. Sci. Mater. Electron.* **2024**, *35*, 308. https://doi.org/10.1007/s10854-023-11913-6.
27. Zhao, L.; Li, L.; Abbas, Z.; Zhang, L.; Deng, J.; Tang, Z.; Su, J. Surface Roughness Effects on Aluminum-Copper Ultrasonic Dissimilar Welds: Interface, Strength, and Failure Analysis. *J. Mater. Eng. Perform.* **2026**, *35*, 23562–23572. https://doi.org/10.1007/s11665-026-13272-9.
28. Helfers, E.; Müller, F.W.; Schiebahn, A.; Reisgen, U. Laser-based surface pretreatment for ultrasonic metal welding of copper and dissimilar aluminium-copper joints. *Weld. World* **2026**, *70*, 1051–1075. https://doi.org/10.1007/s40194-025-02197-x.
29. Zhao, L.; Saboor, H.A.; Tian, Y.; Li, L.; Li, S.; He, S.; Abbas, Z.; Wei, W. Microtopographic, mechanical and microstructural evaluation of ultrasonic torsional welds for Al-Cu electrical connections. *Mater. Des.* **2026**, *264*, 115785. https://doi.org/10.1016/j.matdes.2026.115785.
30. Choudhari, D.; Singh, U.; Kumar, R.; Rajak, A. Influence of welding parameters on bond quality of ultrasonic welded joints for multilayer thin Cu-Al foil stacks. *Weld. World* **2026**. https://doi.org/10.1007/s40194-026-02506-y.
31. Abbas, Z.; Deng, J.; Zhao, L.; Islam, M.S. Surface-conformed approach for mechanical property analysis using ultrasonic welding of dissimilar metals. *Int. J. Adv. Manuf. Technol.* **2024**, *132*, 3447–3466. https://doi.org/10.1007/s00170-024-13538-3.
32. Yang, J.W.; Xie, C.H.; Zhang, J.; Ding, Z.Y.; Qiao, J. An atomic insight into effect of grain boundary on diffusion behavior of Cu/Al dissimilar materials undergoing ultrasonic welding. *J. Iron Steel Res. Int.* **2024**, *31*, 2555–2567. https://doi.org/10.1007/s42243-024-01349-5.

Disclaimer/Publisher's Note: The statements, opinions and data contained in all publications are solely those of the individual author(s) and contributor(s) and not of MDPI and/or the editor(s). MDPI and/or the editor(s) disclaim responsibility for any injury to people or property resulting from any ideas, methods, instructions or products referred to in the content.